Localized orbital theory and ammonia triborane

Joseph E. Subotnik,*[a] Alex Sodt*[b] and Martin Head-Gordon*[c]

Received 18th June 2007, Accepted 13th August 2007
First published as an Advance Article on the web 29th August 2007
DOI: 10.1039/b709171k

In a previous paper [J. Subotnik, Y. Shao and W. Liang, and M. Head-Gordon, *J. Chem. Phys.*, 2004, **121**, 9220], we proposed a new and efficient method for computing localized Edmiston–Ruedenberg (ER) orbitals, which are those localized orbitals that maximize self-interaction. In this paper, we improve upon our previous algorithm in two ways. First, we incorporate the resolution of the identity (RI) and atomic resolution of the identity (ARI) approximations when generating the relevant integrals, which allows for a drastic reduction in computational cost. Second, after convergence to a stationary point, we efficiently calculate the lowest mode of the Hessian matrix in order to either (i) confirm that we have found a minimum, or if not, (ii) move us away from the current saddle point. This gives our algorithm added stability. As a chemical example, in this paper, we investigate the electronic structure (including the localized orbitals) of ammonia triborane ($NH_3B_3H_7$). Though ammonia triborane is a very electron-deficient compound, it forms a stable white powder which is now being investigated as a potential hydrogen storage material. In contrast to previous electronic structure predictions, our calculations show that ammonia triborane has one localized molecular orbital in the center of the electron-deficient triborane ring (much like the single molecular orbital in H_3^+), which gives the molecule added energetic stability. Furthermore, we believe that $NH_3B_3H_7$ is the smallest stable molecule supporting such a closed, three-center BBB bond.

I. Localized orbital theory

Quantum chemists have long understood that there are infinitely many equivalent ways to understand the behavior of individual electrons in a molecule. On the one extreme, the delocalized, canonical molecular orbitals provide an excellent framework for understanding the attachment and detachment of electrons onto or from a molecule, as measured by ionization potential or electron affinity. According to Koopman's theorem,[1] the energies of added or withdrawn electrons correspond roughly to the diagonal matrix elements of the Fock operator in a basis of delocalized, canonical molecular orbitals. On the other extreme, localized orbitals describe well the chemical picture whereby electrons are held either in lone pairs or in bonds between atoms, matching a chemist's intuition of Lewis dot structures with a quantitatively rigorous quantum mechanical approach.[2,3] Even though these two models point out extremely different features of the quantum mechanical behavior of electrons, they are both equally valid, as localized orbitals are merely an orthogonal transformation of canonical orbitals.[4]

Beyond these two extreme, but valid, pictures of single electron behavior, there are obviously many more. Certain physical properties are best analyzed in terms of partially localized orbitals somewhere in between, which are encountered as one transforms continuously from canonical to localized orbitals. For instance, suppose we want to model charge transfer between molecules A and B which are in close contact. For such a test case, the natural electronic orbitals should be delocalized, but over only one of the monomers (A or B, not both). Thus, choosing the most natural orbitals for a given physical problem is non-trivial, and theoretical chemists need as many tools as possible available for describing one-electron orbitals in a chemically meaningful way.

This article focuses on fully localized electronic orbitals which are found by optimizing one of the three functions below:

$$\zeta_{\mathrm{ER}}(\eta_1, \ \cdots \ , \eta_n) = \sum_i \left\langle \eta_i \eta_i \left| \frac{1}{r} \right| \eta_i \eta_i \right\rangle \qquad (1)$$

$$\zeta_{\mathrm{Boys}}(\eta_1, \ \cdots \ , \eta_n) = \sum_i |\langle \eta_i | \boldsymbol{r} | \eta_i \rangle|^2 \qquad (2)$$

$$\zeta_{\mathrm{PM}}(\eta_1, \ \cdots \ , \eta_n) = \sum_{i=1}^{n} \sum_{A=1}^{\mathrm{Numb.Atoms}} |\langle \eta_i | P_{\mathrm{A}} | \eta_i \rangle|^2 \qquad (3)$$

The first function (labeled ER) defines the Edmiston–Ruedenberg[5] orbitals by maximizing the self-interaction of the localized orbitals. The second function defines the Boys orbitals by maximizing the sum of the distances between the centroids of the localized orbitals.[3,5,6] Finally, the Pipek–Mezey orbitals[7] are defined by the third function in terms of maximizing the square of the projection onto individual atomic orbitals. Here, P_{A} projects a given orbital onto the space of atomic orbitals centered at atom A.

[a] *Biophysics Program, University of California, Berkeley, CA 96720. E-mail: subotnik@post.harvard.edu*
[b] *Department of Chemistry, University of California, Berkeley, CA, 94720. E-mail: alexsodt@berkeley.edu*
[c] *Chemical Sciences Division, Lawrence Berkeley National Laboratory, Berkeley, CA, 94720. E-mail: mhg@chem.berkeley.edu*

Of the three different localization schemes, ER orbitals are arguably the most chemically meaningful. First, ER orbitals usually preserve σ–π separation,[7] much like PM orbitals, but unlike Boys orbitals. Second, ER orbitals (like Boys orbitals, but unlike PM orbitals) are defined intrinsically, without reference to any atomic orbital basis. Third, ER orbitals (unlike Boys and PM orbitals) take into account both the distances between centroids and the spatial extent of any given orbital. For this reason, early work on chemical bonding (especially, the boron work of W. Lipscomb and co-workers[8,9]) focused on the ER orbitals, as will we in this paper.

Until recently, ER orbitals could not be calculated in a reasonable amount of time. According to the original Edmiston and Ruedenberg prescription,[5,10] which was followed for forty years, one computes ER orbitals following an algorithm that scales formally as N^5 and runs along so-called "Jacobi sweeps." This approach precluded computing ER orbitals for large systems, and led many researchers to switch from computing ER orbitals to Boys orbitals.[10,11] Recently, however, two of the present authors suggested a new DIIS-based algorithm which was linear scaling in principle, and we showed in 2004 that this algorithm did lead to a large savings in computational time,[12] which has renewed interest in the ER orbitals.[13] Nevertheless, our original algorithm had two flaws. First, though the matrix elements $(\eta_i\eta_i|\eta_j\eta_j)$ could be computed in a linear fashion, the prefactor remained large, and the time for localization still dwarfed the SCF time for large systems (see below). Second, the original algorithm suffered from convergence errors, caused by convergence to saddle points (rather than minima) of the ER function. Absolute convergence forced one to build and explicitly diagonalize the second-derivative. In the case of benzene interacting with NO_2 or NO,[14] we found several saddle points in navigating between the Boys localized orbitals and ER localized orbitals.[12]

These two problems have now been remedied. First, in order to quickly compute matrix elements $(\eta_i\eta_i|\eta_j\eta_j)$, the resolution of the identity (RI)[15,16] and atomic RI (ARI)[17] approximations are invoked. The RI-approximation allows one to fit the product of pairs of orbitals in terms of a single set of auxiliary orbitals with large angular momenta. With an appropriate auxiliary basis,[16,18] the RI-approximation regularly reduces computational cost by an order of magnitude, and errors are usually only on the order of 10–30 μH per second-row atom.[17] The ARI approximation of Sodt *et al.*[17] is a further approximation which combines the RI approximation with locality for the speediest possible implementation. For the Coulomb matrix, errors are usually very similar to those of full-RI,[17] perhaps 1–5 μH larger. These approximations allow the computation of localized ER orbitals in a time far smaller than the HF time. See section II for algorithmic details, and section IV for numerical results.

Second, an efficient algorithm (requiring only quadratic memory) has been implemented to calculate the most negative mode of the second-derivative of the ER-function. This has been accomplished by applying the Davidson algorithm[19–21] to functions defined on the space of rotations (*i.e.* the orthogonal group). See section III for more details. Using second-derivative information when computing ER orbitals, we follow the ideas of Pople and Seeger[22] to ensure that we converge to minima (rather than saddle points). There remains the problem of multiple minima. For certain molecules and localizing functions, (*e.g.* the ER orbitals for benzene), there is a continuous degeneracy of localized orbitals, not one being unique,[12] but all being equivalent. For other molecules, one has multiple discrete minima, caused by symmetry.[23] These localized orbitals can be equivalent or different. When these localized orbitals are non-equivalent (*e.g.* B_5H_9), Lipscomb suggests using randomly generated initial guesses in order to find all of the different solutions, as they are all physically meaningful.[23] The problem of multiple minima when localizing molecular orbitals is non-trivial, and convergence to local minima is not only unavoidable, but also can be chemically meaningful.

Finally, in section V, we have employed this new algorithm to compute the localized orbitals of ammonia triborane ($NH_3B_3H_7$). Ammonia triborane is currently being investigated for its potential as a carrier of hydrogen for industrial fuel cells. For it to be viable, it is necessary to understand how one can most easily hydrolyze ammonia triborane and recycle the borate leftovers. Understanding the electronic structure and properties of $NH_3B_3H_7$ is a necessary first step towards controlling and manipulating the molecule's chemical reactions.

II. RI methods

For large molecules, a standard implementation of the new DIIS-based algorithm is limited by the ability to form the R-matrix $R_{ji} = (\eta_j\eta_j|\eta_j\eta_i)$. Formally, this is a quintic step. We showed previously[12] that such a matrix could be formed in linear time using exact methods[24] if we invoke the fact that η are local orbitals. The prefactor for this construction was large, however, and for moderately sized molecules, the localization was still far slower than the HF algorithm. For instance, for the alkane $C_{60}H_{122}$ using the most sparse basis possible (a STO-3G basis), the time for constructing $(\eta_i\eta_i|\eta_j\eta_j)$ was 65 s compared with 36 s for each SCF step (as performed on an IBM RS/6000).

So-called "resolution of the identity" (RI) algorithms are ideal for constructing small sets of transformed Coulomb integrals from a large number of four-center AO basis integrals. An extreme example of this is the molecular self Coulomb interaction, $(\rho|\rho)$, with speed-ups in the tens even for small basis sets (where RI algorithms are least suited).[17,25,26] Similarly, generalized valence bond methods such as perfect pairing require small sets of valence space MO integrals and see enormous speed-ups.[27] For this reason, we have implemented an efficient algorithm for computing ER orbitals based on the atomic RI (or ARI) approximation. We will now describe exactly how our algorithm works both (i) in words and (ii) in the form of a computational flowchart.

The RI algorithm requires specification of a fitting basis set,[16,18] which is traditionally of the same atom-centered Gaussian form as the orbital basis set. Fits to orbital products (such as $\mu(r_1)\nu(r_1)$ or $\eta_i(r_1)\eta_j(r_1)$) are computed as linear combinations of the fitting basis functions. The fits are chosen

to minimize the self-Coulomb interaction of the fit error

$$\iint (\eta_i(r_1)\eta_j(r_1) - \widetilde{\eta_i(r_1)\eta_j(r_1)}) \frac{1}{|r_1 - r_2|} (\eta_i(r_2)\eta_j(r_2) - \widetilde{\eta_i(r_2)\eta_j(r_2)}), \quad (4)$$

where

$$\widetilde{\eta_i(r)\eta_j(r)} = \sum_P C_{ij}^P P(r), \quad (5)$$

and $P(r)$ is an atom-centered fitting function. The fitting coefficients that minimize this simple quadratic form (in the variable P) are

$$C_{ij}^P = \sum_Q (P|Q)^{-1}(Q|\eta_i\eta_j) \quad (6)$$

where $(Q|\eta_i\eta_j)$ is the Coulomb interaction of $Q(r_1)$ with $\eta_i(r_2)\eta_j(r_2)$. Integrals are then evaluated as

$$(\eta_i\eta_j|\eta_j\eta_j) = \sum_P C_{ij}^P (P|\eta_j\eta_j), \quad (7)$$

for example. We note that this expression is not unique. For example, one can instead use

$$(\eta_i\eta_j|\eta_j\eta_j) = \sum_{P,Q} C_{ij}^P (P|Q) C_{jj}^Q. \quad (8)$$

Eqn (7) and (8) are equivalent so long as one has used eqn (6) to obtain fit coefficients.

If we apply the RI approximation to orbital localization, we are forced, in the course of such a procedure, to compute new integrals between orbitals that are steadily rotated one into the other (mixing only occupied orbitals between themselves). In this case, from one iteration to the next (η_i' to η_i) the fits may be transformed as

$$C_{i\mu}^P = \sum_{i'} C_{i'\mu}^P X_{i,i'}, \quad (9)$$

where $X_{i',i}$ transforms from the previous set of occupied orbitals to the next, and μ is an atomic orbital basis function. In other words, we do not need to reform fits from eqn (6) at every iteration, a fact which saves us time. Afterwards, we form the fully transformed fits

$$C_{ij}^P = \sum_\mu C_{i\mu}^P X_{j,\mu} \quad (10)$$

Thus, the RI approximation can be invoked to efficiently generate fitting coefficients in the course of an orbital localization subroutine, and these coefficients can be contracted in order to form the final set of integrals using eqn (8).

For even more efficiency than the standard RI approach, the ARI procedure of Sodt *et al.* forms compact fits of $\mu(r)\eta_i(r)$. The ARI algorithm generates fits of $\mu(r)\eta_i(r)$ using only fitting functions (P) which are near μ. It does this in such a way that the fit changes continuously and differentiably with nuclear coordinates. One key insight behind the ARI procedure is to note that when orbital products are fit only locally, we must invert the overlap matrix of only a local auxiliary basis, which can be made linearly scaling. Without local approximations, we would be forced to invert a non-sparse Coulomb-overlap matrix and do cubic work. Thus, ARI rapidly speeds up our calculations, and we refer the interested reader to the cited work[17] for further details. Furthermore, in the case of computing ER integrals, we note that ARI is an ideal technique because (i) it eliminates the cubic storage of retaining $C_{i\mu}^P$ between iterations (because we force μ to be close to P); and (ii) it reduces the bottleneck fitting step (eqn (6)) an order of scaling (because the number of fitting functions is constant for large enough systems). The fit's storage footprint is quadratic if we ignore the locality of η_i (and compute the fit of all $\mu(r)\eta_i(r)$). One potentially needs only a linear amount of memory if one does invoke such locality.

When using an ARI fit, eqn (7) is no longer equivalent to eqn (8) (because we are using locality to approximate $(P|Q)^{-1}$ in eqn (6)). Eqn (8) is the computationally efficient choice (rather than eqn (7)), and, for that reason, we have implemented an ARI algorithm with eqn (8) below. One further detail is that (with ARI), C_{ij}^P must be symmetrized as $\frac{1}{2}(C_{ij}^P + C_{ji}^P)$ to properly compute orbital derivatives of $(\eta_j\eta_j|\eta_j\eta_j)$.

We sum up our ARI-based algorithm with a step-by-step flowchart shown in Fig. 1. Steps 1–4 need only be performed once. Step 2 is asymptotically linear scaling, because only those Q and ν near μ must be considered. Steps 3 and 4 are asymptotically quadratically scaling (if the initial orbitals are not local), as every quantity (P, Q, ν) must be near μ to be significant. We do not take advantage of orbital locality in our implementation (although orbital locality greatly accelerates the step-wise convergence of our algorithm as discussed in ref. 12.) Steps 5 and 7 scale cubically without fast Coulomb methods or orbital locality. However, two indices in Step 5 are quite small (the size of the orbital localization space), and both steps are implemented as efficient matrix multiplies. Steps 6, 8, and 9 are computationally trivial in comparison.

III. Second-derivative tests

The 2004 algorithm[12] had the tendency to converge to saddle points: the algorithm locates points in rotation space for which the derivative is zero, but there is no stipulation on the eigenvalues of the second-derivative matrix. In order to ameliorate this problem, we have implemented an algorithm to check for the lowest eigenvalue of the Hessian matrix after convergence. Formally, if we parameterize the group of rotations by the antisymmetric algebra, $\boldsymbol{U} = e^{\boldsymbol{A}}$, the second derivative of the ER function can be written down as follows

$$\frac{\partial^2 \zeta_{\mathrm{ER}}}{\partial \Delta_{pq} \partial \Delta_{rs}}|_{\Delta=0} = T_{rqps} + T_{psrq} - T_{qspr} - T_{prqs}$$

$$T_{rpqs} = \{2(ps|ss) + 2(sp|pp) - 4(ps|qq) - 8(pq|sq)\}\delta_{rq} \quad (11)$$

Formally, this quantity is quartic in size. In order to identify the smallest or most negative eigenvalue of the Hessian, we have implemented the Davidson diagonalization procedure[19–21] in a manner which requires only a quadratic amount of memory. Given a matrix operation A and a subspace V, the

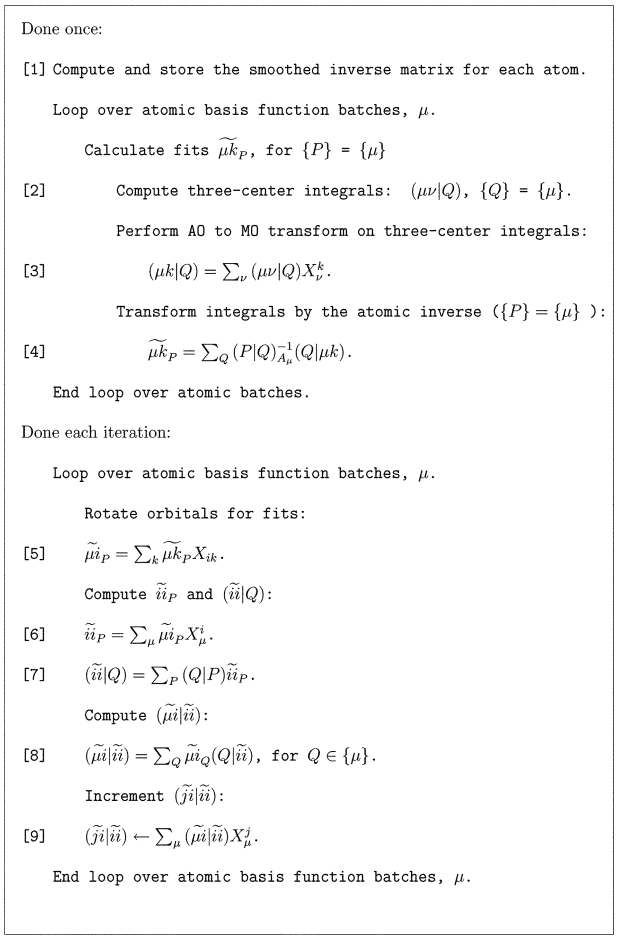

Fig. 1 The algorithm for computing Coulomb integrals $(ji|ii)$. The notation $\{P\}$ indicates a set of fitting functions, P, and $\{\mu\}$ indicates the set of fitting functions which are within the fitting radius of the atom to which μ belongs. Items labeled by a number in square brackets are computational steps referred to in the text. Greek letters refer to atomic orbitals, and Roman letters refer to molecular orbitals. k refers to the initial guess orbitals; i, j refer to variable, localized orbitals which are changing during the course of the minimization. X refers to an orbital transformation.

Davidson algorithm iteratively expands the subspace V by looking for the appropriate vector $x \in V$, and then considering Ax. The algorithm converges when x approaches the correct eigenvalue. For an excellent review, see ref. 21.

As a practical matter, during an ER calculation, if the Hessian matrix has a negative eigenvalue, we follow the procedure of Seeger and Pople[22] (which was prescribed originally for converging to the correct Hartree–Fock ground state, rather than a saddle point). According to the prescription of Seeger and Pople, for the HF case, one solves the problem of saddle points by:

1. Converging to a valid solution.

2. Computing and diagonalizing the second-derivative of the defining function at the converged point, seeking the most negative mode.

3. If we have found a saddle point, pushing off towards the optimum solution and beginning the cycle all over again.

Similarly, in our case, we do one line search in the direction of the eigenvector corresponding to the most negative eigenvalue. Hoping that this line search has moved us into the basin of the minimum for localized orbitals, we then begin our localization algorithm again.

This combination of our algorithm, followed by occasional line searches, has proven to be stable and has consistently ensured that we converge to minima of the ER function (and not saddle points). Although we can never be sure that we are finding the global maximum, one can explore such a possibility by varying the initial guess for the localized orbitals. Starting from different initial guesses for the ER orbitals should find different, local minima if they exist. Certainly, changing the initial guess forces one to encounter a variety of different saddle points in the course of a calculation. Furthermore, as discussed in the Introduction, equivalent multiple minima are inevitably caused by symmetry requirements;[23] and non-equivalent multiple minima can be chemically meaningful (at least in the case of boron compounds), rather than computational inconveniences.[23]

IV. Numerical results

The algorithms described above have been implemented into the Q-Chem[28] quantum chemistry package. Table 1 details the computational expense of the ARI-based ER optimization for a system of graphite-like molecules of increasing size: benzene (1 ring of 6 carbons, C_6H_6), coronene (7 rings of 6 carbons glued together, $C_{24}H_{12}$) and circumcoronene (19 rings of 6 carbons glued together, $C_{54}H_{18}$). The localized orbitals of this series of molecules are quite interesting and will be described in a future publication. The basis set is cc-pVDZ, the initial guess for localized ER orbitals are the Boys orbitals, convergence is defined by the criteria $\max(R_{ij} - R_{ji}) < 10^{-5}$, and all calculations were run on a single 2.2 GHz Apple XServe G5 processor.

Not listed in Table 1 is the initial cost of computing the fit to μi, which must be done only once and is typically much smaller than the total expense (63 s *vs.* 13 216 s for circumcoronene). Compared with the full RI approximation, ARI is typically cheaper by a factor of $X_{\text{near}}/X_{\text{total}}$, where X_{near} is the typical number of nearby fitting functions, and X_{total} is the total

Table 1 Details of the computational expense for calculating ER orbitals. A single ER step compares extremely favorably with a single SCF step, yet ER optimization requires many more iterations. Yet even for a complicated optimization with eighteen encountered saddle points, ER optimization time is comparable to the SCF time. All calculations were run on a single 2.2 GHz Apple Xserve G5 processor

System	Fock build	$(ii\|ij)$ time	$(ii\|jk)/(ii\|ik)$ time	Steps	Saddle points	Total ER time	Total SCF time
Benzene	3.43	0.03	0.06	37	1	8.08	26.14
Coronene	150.82	1.00	5.50	42	1	138.33	1108.02
Circumcoronene	1003.70	7.84	88.35	807	18	13 216.13	7319.44

number of fitting functions. For circumcoronene, the value of X_{near} for a carbon in the interior of the ring is 560, while the total number of fitting functions is 3276. Additionally, the ARI approximation has a smaller storage footprint by the same factor. For the two smaller systems studied, benzene and coronene, only one saddle point was encountered, and the orbital optimization took relatively few iterations, yielding ER times much smaller than the total SCF time. However, for circumcoronene, eighteen saddle points were encountered, and as a result the ER time exceeded the SCF time. With an improved minimization algorithm, it is possible that the number of minimization steps could be reduced. Additionally, it is possible that a smaller fitting basis set or reduced ARI fitting radius could be used initially, with further refinement pursued in a larger fitting space.

With the somewhat less accurate functional (eqn (8)) and small fitting radius used (4 a.u.) the accuracy of $(\eta_i\eta_i|\eta_i\eta_j)$ construction is worth investigating. For each system in Table 1, we took the converged ER orbitals with fitting radius 4 (a.u.), and refined them with fitting radius 6. Additional change was minimal: no further saddle points were encountered, even for circumcoronene, and navigating from the localized orbitals found with a 4 a.u. cutoff to those for the 6 a.u. cutoff required fewer than 6 steps in all cases. Thus, though the accuracy of $(\eta_i\eta_i|\eta_i\eta_j)$ construction may indeed be rough, we believe it to be sufficient to obtain ER orbitals of high enough quality for any qualitative chemical analysis. Admittedly, though, local correlation algorithms[29] will depend more carefully on the tails of the localized orbitals and require more accurate fits.

V. Chemical example: ammonia triborane

Ammonia triborane ($NH_3B_3H_7$) is a nitrogen borane derivative made up of a three-boron-ring cluster, with one nitrogen atom covalently bonded to one of the three borons above the plane of the boron atoms. Recent interest in $NH_3B_3H_7$ has focused on the molecule's capacity to store hydrogen for a hydrogen-powered economy.[30] $NH_3B_3H_7$ is stable and very soluble in water, not terribly O_2 sensitive,[31] and hydrolyzes only in the presence of either a metal catalyst or an acidic environment. The stoichiometry of ammonia triborane hydrolysis is as follows

$$NH_3B_3H_7(s) + 6H_2O(l) \rightarrow NH_4^+(aq) + 3BO_2^-(aq) + 2H^+(aq) + 8H_2(g) \qquad (12)$$

Because the weight fraction of H_2 liberated is so great (in practice, it can be as large at 6%), Yoon and Sneddon have argued that the properties of $NH_3B_3H_7$ should be thoroughly investigated. Recently, the authors have reported an efficient method for its synthesis.[30] We now explore the electronic structure of ammonia triborane, hoping that our analysis may help to manipulate $NH_3B_3H_7$ as a potential hydrogen storage media.

The optimized geometry we have found for $NH_3B_3H_7$ differs significantly from the original crystallographic results reported by Nordman and Reimann[32] in 1959. Beginning with the experimental crystal structure, we have minimized the energy computationally at the RI-MP2/cc-pVTZ (frozen core) level of theory. We find that the crystal structure changes not insubstantially, moving from the asymmetric 1959 crystal structure to a symmetric geometry with a plane of reflection perpendicular to the B2–B3 bond. A three dimensional image of our optimized geometry is provided in Fig. 2. We find no other stable geometries whatsoever—for a wide variety of starting geometries, we always reach the same optimized geometry as in Fig. 2. While the positions of hydrogen atoms in a crystal structure are always difficult to ascertain, the difference in the B–N bond distance (experimentally 1.58 Å, theoretically 1.62 Å) was larger than expected.

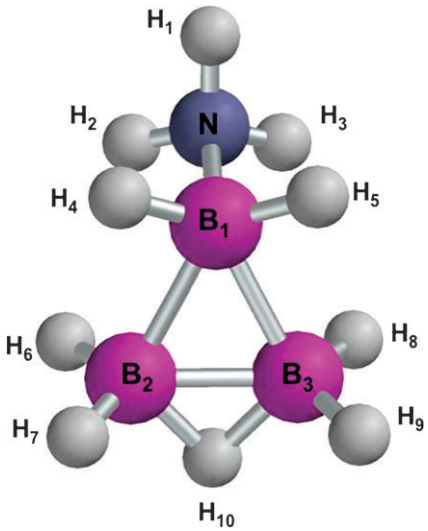

Fig. 2 The optimized nuclear geometry of ammonia triborane.

Recently, Dixon and co-workers[33] have used standard high level electronic structure methods to investigate the mechanism whereby hydrogen is released from ammonia triborane. Following the lead of W. Lipscomb and others,[8–10,23,34] we have computed the localized ER orbitals for the compound (starting from the canonical HF orbitals). A simple count of electrons and bonds in Fig. 2 shows that, ignoring the octet rule, the molecule appears to have 15 nominal bonds or 30 electrons. At the same time, however, an elementary count of electrons reveals that there are only 24 electrons to go around. Our calculations show that the distribution of the valence electrons into localized ER orbitals follow the patterns observed by the Lipscomb group, which found that, in addition to standard pairwise covalent bonds, for boron complexes, one also expects (i) open two-center BHB bonds, and (ii) closed, three-center BBB bonds.[23]

With one exception (any bond touching H10), all heavy atom–hydrogen bonds appear to be ordinary pairwise-sigma bonds, as usual. This accounts for 18 electrons. As would be expected, the nitrogen–boron bond is a dative covalent bond, with nitrogen donating two electrons to the B–N bond. We have now accounted for 20 electrons. More interestingly, at the bottom of the molecule, borons B2 and B3 share two electrons which are delocalized over the two-center B2–H10–B3 bond. This BHB electronic orbital is very similar to that found in diborane (B_2H_6).[35] At this point, only two electrons remain and each boron atom has only six electrons in

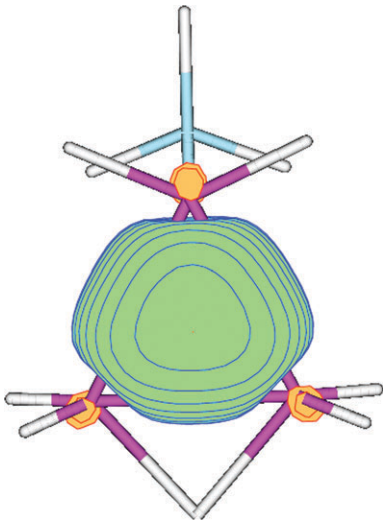

Fig. 3 The ring-centered localized electronic orbital of ammonia triborane.

its valence shell. In order to best achieve charge balance and satisfy the octet rule, the remaining two electrons (alpha and beta) are localized in the center of the triborane ring, and are shared by each of the three boron atoms (see Fig. 3). This is a closed, three-center BBB bond as discussed by Lipscomb.[23] We believe that $NH_3B_3H_7$ is the smallest stable compound demonstrating such a bond. This ring-centered electron resembles the alpha and beta orbitals found in an elementary calculation of H_3^+, a classic example of a charge-deficient molecule, and helps to explain the chemical stability of $NH_3B_3H_7$ *versus* other small boranes.

The electronic structure presented here disagrees with the predictions of Nordman and Reimann.[32] Given the asymmetry of the experimental crystal structure, they anticipated that the triborane ring was held together by (i) a BHB bond between B2–H10–B3, (ii) a BHB bond between B2–H4–B1, and (iii) a regular B1–B3 bond. Though they allowed for the possibility of a Lipscomb-like BBB bond, the authors supposed it unlikely given the high asymmetry of their crystal structure. Now, for one small borane complex (B_5H_9), Lipscomb did find more than one set of non-equivalent localized ER orbitals for the molecule (as shown in Fig. 4) and noted that these orbitals were not always symmetric.[23] Lipscomb argued that both representations were physical, and that in order to reach both solutions, one should be begin several different ER localization calculations with different starting guesses. Therefore, we note that in the course of our HF and DFT calculations, we have generated a variety of randomized initial guesses for the ER orbitals (after the SCF calculation) by multiplying the Boys orbitals by smaller, random orthogonal matrices. We always find only one set of ER orbitals (which have a central BBB bond). We never find the localized orbitals predicted by Nordman and Reimann.

A comparison of $NH_3B_3H_7$ with NH_3BH_3 appears quite relevant for understanding how a metallic catalyst or an acid drives the dehydrogenation of $NH_3B_3H_7$. On the one hand, the two molecules are very similar. Both molecules have a crystalline N–B bond distance of 1.58 Å.[32,36] And at the RI-MP2/cc-pVTZ (frozen core) level of theory, one can calculate their bond distances in vacuum to be 1.62 Å for $NH_3B_3H_7$ and 1.65 Å for NH_3BH_3. On the other hand, the charge distributions (arising from charge transfer from NH_3 to the boron functional group) are different. The dipole moment (at the HF cc-pVTZ level) is computationally 5.4 D for NH_3BH_3 and 6 D for $NH_3B_3H_7$. The experimental number is 5.2 D for NH_3BH_3.[37–39] There is no experimental number for $NH_3B_3H_7$.

Dixon and co-workers[40] have argued that, in the case of NH_3BH_3, acid-catalyzed dehydrogenation purportedly begins by attack of a proton on a hydrogen bonded to boron, liberating H_2 gas:

$$H^+ + NH_3BH_3 \rightarrow H_2 + NH_3BH_2^+ \qquad (13)$$

If we consider this reaction in gas form in a vacuum environment, the difference in electronic energy between NH_3BH_3 and $NH_3BH_2^+$ (calculated by RI-MP2 in a cc-pVTZ basis with core frozen) is 543 kcal mol^{-1}. If one models the Hamiltonian using the rigid rotor and harmonic approximations[41] to account for zero-point energy, rotations, vibrations and translations, one finds a difference in enthalpy of 537 kcal mol^{-1} at 298 K. Though these absolute numbers are not meaningful without a reasonable model for the chemical form of the proton donor, they can be meaningfully compared to the parallel numbers for $NH_3B_3H_7$. For $NH_3B_3H_7$, one finds that the H_2-extracted cation with the lowest energy has the

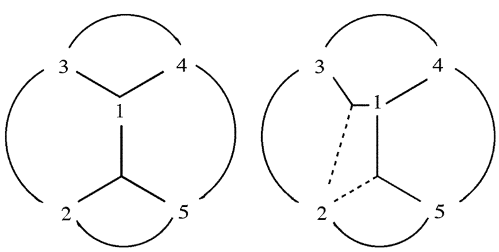

Fig. 4 The two non-equivalent localized orbitals of B_5H_9. Here, each numeral stands for a BH group. The curvy bonds on the outside represent three-center BHB bonds. The dashed line represents a partial bond. See ref. 23. For $NH_3B_3H_7$, we find only one unique set of localized ER orbitals.

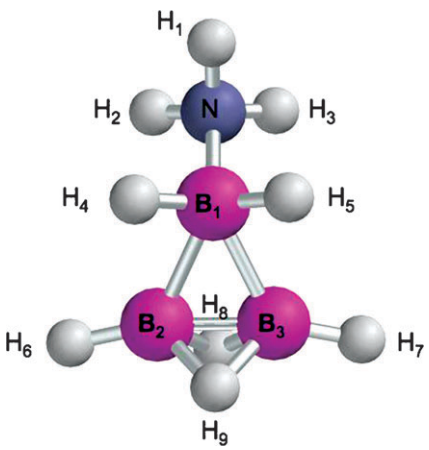

Fig. 5 The optimized nuclear geometry of ammonia triborane after extraction of a hydride ion ($NH_3B_3H_6^+$).

structure shown in Fig. 5. The difference in electronic energy between $NH_3B_3H_7$ and $NH_3B_3H_6^+$ is 538 kcal mol^{-1}, or 531 kcal mol^{-1} if one includes enthalpic effects. The similarity of these absolute numbers suggest that $NH_3B_3H_7$ may be dehydrogenated *via* a mechanism not too dissimilar from that of NH_3BH_3. This parallelism may end, however, when one considers the reaction in aqueous solution (or a condensed environment more generally). In such a case, the larger dipole moment of ammonia triborane may play a bigger role, and more elaborate calculations are necessary to be more definitive.

VI. Discussion

This article has focused on computing localized orbitals using advanced tricks from electronic structure theory, assuming that the physical meaning of ER orbitals can be taken for granted. Before concluding, however, several comments should be offered about when localized occupied orbitals are chemically and physically meaningful constructions—and when they are merely mathematical curiosities.

On one extreme, for neutral, closed shell, second-row molecules which have simple Lewis dot structures and obey the octet rule, localized orbitals clearly correspond to lone pairs or bonding orbitals. Obviously, these are extremely physical representations of electronic behavior. On the other extreme, as we have stressed in previous publications,[42] the localized orbitals of a general virtual space are not at all physically meaningful. The virtual orbitals most often are just the leftovers of the large function space once the occupied space has been extracted. In particular, a localization function has a rugged potential surface, with many, many minima, when applied to a virtual space.[42,43]

Most interesting chemical examples fall somewhere in between these two extremes, and the divide is not strictly between occupied and virtual orbitals. On the one hand, localized occupied orbitals are sometimes not meaningful. For instance, suppose one considers the localized occupied orbitals of an anionic, long, conjugated organic molecule (with one extra electron in the alpha space). In that case, if one rotates and mixes all of the $(N + 1)$ alpha electrons and all N beta electrons to form the most localized representation, the result is rather meaningless as the N lowest energy localized alpha electrons no longer correspond to the N localized beta electrons. Instead one must consider the N corresponding alpha and beta electrons, localize these corresponding spaces, and leave alone the $(N + 1)$st electron (which usually occupies a particle-in-a-box like state). One cannot freely localize the entire occupied space and expect meaningful chemistry. On the other hand, there are meaningful localized virtual orbitals. As we have argued previously on the basis of perfect-pairing calculations,[44–47] and then demonstrated,[42] if one considers the virtual orbitals from a HF calculation performed in a minimal basis, these so-called valence virtual orbitals are very meaningful after localization. They are essentially anti-bonding orbitals. Thus, both occupied and virtual spaces can have meaningful and meaningless localized orbitals, and we must look elsewhere for an answer.

The case of ammonia triborane is a good example to consider in the context of discerning when localized orbitals are meaningful. In general, for occupied orbitals, a large array of chemical literature (beginning with the work of W. Kohn) has investigated the decay of the density matrix and, hence the localized orbitals, in periodic potentials.[48,49] The set of localized orbitals may decay no faster than the one-particle density matrix, suggesting that the decay of the density matrix is a rigorous quantifier of the locality of a set of electronic orbitals. Unfortunately, no general results have yet been derived for non-periodic potentials, and one must extrapolate the results of Kohn, Arias and others to super-cells when applying them heuristically to molecules. For insulators (with direct gap Δ), the density matrix decays exponentially in space: $\rho(r,r') \sim e^{-\gamma|r-r'|}$. In the weak-binding limit, $\gamma \sim \Delta$, while in the tight-binding limit, there is no general rule. (In his work on one-dimensional, centrosymmetric potentials, Kohn found $\gamma \sim \Delta^{1/2}$.) For non-periodic potentials (*e.g.* a molecule in vacuum), the decay of localized occupied orbitals is less certain. If, however, the energy of the HOMO is sufficiently negative with respect to the vacuum, and if the HOMO–LUMO gap is large enough, then the density matrix should decay exponentially and there will exist meaningful localized orbitals, as we find for ammonia triborane.

One interesting characteristic of ammonia triborane is that there exists a unique partial or fractional Lewis dot structure for the molecule, which captures the BBB and BHB bonds. To our knowledge, there is no clear correspondence between the band gap criterion and Lewis dot structures. On the one hand, clearly there exist some insulators for which Lewis dot structures do not exist. On the other hand, there are many insulators for which *many* "resonant" Lewis dot structures exist. For a given molecule, can we relate mathematically the number of resonant Lewis dot structures to the decay of the density matrix, and in turn to the localized orbitals—do multiple minima of the localization function reliably correspond to multiple resonant structures? We cannot answer this question, but the case of ammonia triborane suggests that fractional Lewis dot structures connect strongly to the structure of localized electronic orbitals.

Regarding the virtual space, localized virtual orbitals are physically meaningful when they arise from calculations in a minimal basis, where the energy is low and they can be interpreted as antibonding orbitals.[42] For the case of $NH_3B_3H_7$ we show in Fig. 6 a localized, valence virtual orbital which has been created using the techniques of ref. 42 and substituting the ER function for the Boys function. This localized virtual orbital (which is directed along the B1–B3 axis with a node midway) comes in a group of two, with its counterpart running along the B1–B2 axis, and it is the most delocalized of all of the valence virtuals of ammonia triborane. As judged by location and extent, this localized orbital interacts more with the central BBB orbital than any other virtual orbital. Thus, we expect correlations involving this localized virtual orbital to contribute significantly to the correlation energy of the ground state (within the context of a local correlation theory[29]). Furthermore, as the B2–B3 bond is dissociated, we expect this anti-bonding orbital to become more occupied.

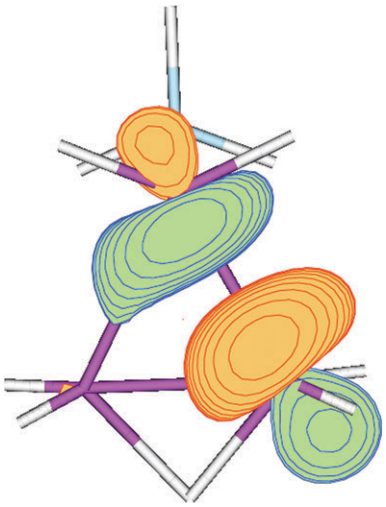

Fig. 6 The localized valence-virtual orbital of ammonia triborane which is most delocalized. This valence virtual orbital is the virtual orbital which overlaps most strongly with the occupied BBB orbital.

Finally, the introduction to this article discussed how, for charge transfer, the most revealing localized orbitals would be intermediate between the canonical orbitals and the most localized orbitals. The canonical orbitals are those delocalized orbitals for which the Fock matrix is diagonal in their basis, while in a basis of localized orbitals, the Fock matrix is certainly not diagonal (although it decays away from the diagonal). More than twenty years ago, Kapuy and co-workers wondered if, starting from delocalized canonical orbitals, it might be possible to construct localized orbitals for which the Fock-matrix was still diagonal dominant.[50–53] Such orbitals would be intermediate between the canonical orbitals and the most localized orbitals, and for the purposes of Kapuy *et al.*, they would be very useful in many local correlation schemes.[43,54] From an analytical point of view, however, such orbitals might also be very physically meaningful. Let us consider the case of a closed-shell anion which is in a transition state structure, ready to approach a target and donate a pair of electrons into a dative bond. In this case, similar to the case of a radical, our intuitive picture corresponds to N restricted, localized alpha and beta orbitals, and one single pair of delocalized alpha and beta orbitals. We note that this delocalized orbital pair is usually significantly higher in energy than the other, more tightly held electrons—and this property, of course, makes this pair of electrons more likely to attack the target molecule. In the future, theoretical chemists should investigate whether one may construct a localizing scheme that takes into account not just electron position, but also the energy of the canonical orbitals that are mixing, in order to capture the most physical orbital picture. Unfortunately, no elegant algorithm for constructing such orbitals has yet been achieved.[43]

VII. Conclusion

Localized orbitals continue to be an attractive method for understanding the electronic structure of molecules and, in this paper, we have presented a fast algorithm for computing localized ER orbitals which is (i) fast—usually as fast or faster than a traditional HF calculation—and (ii) stable. First, the computational speed for this new algorithm has been greatly increased by the introduction of RI methods, and for treating moderately sized molecules, there is no longer a computational bottleneck in computing localized ER orbitals. Second, the stability component of our algorithm comes from checking the lowest eigenvalue of the second-derivative matrix of the localization function after convergence, ensuring that we reach a minimum. Occasional convergence to saddle points had been problematic for our previous algorithm as demonstrated by the examples of graphite-like materials.

Using the tools above, we have computed and presented in this paper the canonical and localized molecular orbitals of ammonia triborane. We believe that $NH_3B_3H_7$ is the smallest stable molecule that supports a closed BBB bond, and from the data in section V, we speculate that acid-catalyzed dehydrogenation for $NH_3B_3H_7$ proceeds by a mechanism similar to that proposed for NH_3BH_3.[40]

Acknowledgements

We thank Ryan Steele for useful discussions. JES was supported by the Fannie and John Hertz Foundation. This work was supported by the Department of Energy through the Computational Nanosciences program and by the Department of Energy through grant no. DE-FG36-O5G015002. MHG is a part owner of Q-Chem.

References

1 T. A. Koopman, *Physica*, 1933, **1**, 104.
2 J. E. Lennard-Jones and J. A. Pople, *Proc. R. Soc. London, Ser. A*, 1950, **202**, 166.
3 S. F. Boys, *Rev. Mod. Phys.*, 1960, **32**, 296.
4 K. Ruedenberg, in *Istanbul Lectures on Quantum Chemistry*, ed. O. Sinanoglu, Academic Press, New York, 1965, vol. I, p. 85.
5 C. Edmiston and K. Ruedenberg, *Rev. Mod. Phys.*, 1963, **35**, 457.
6 S. F. Boys, in *Quantum Theoory of Atoms, Molecules and the Solid State*, ed. P. Lowdin, Academic Press, New York, 1966, p. 253.
7 J. Pipek and P. G. Mezey, *J. Chem. Phys.*, 1989, **90**, 4916.
8 E. Switkes, W. N. Lipscomb and M. D. Newton, *J. Am. Chem. Soc.*, 1970, **92**, 3847.
9 I. R. Epstein, D. S. Marynick and W. N. Lipscomb, *J. Am. Chem. Soc.*, 1973, **95**, 1760.
10 D. A. Kleier, T. A. Halgren, J. H. Hall and W. N. Lipscomb, *J. Chem. Phys.*, 1974, **61**, 3905.
11 D. A. Dixon, D. A. Kleier, T. A. Halgren, J. Hall and W. N. Lipscomb, *J. Am. Chem. Soc.*, 1977, **99**, 6226.
12 J. E. Subotnik, Y. Shao, W. Liang and M. Head-Gordon, *J. Chem. Phys.*, 2004, **121**, 9220.
13 F. Aquilante, T. B. Pedersen, A. S. de Meras and H. Koch, *J. Chem. Phys.*, 2006, 174101.
14 P. M. Esteve, J. W. W. Carneiro, S. P. Cardoso, A. G. H. Barbosa, K. K. Laali, G. Rasul, G. K. S. Prakash and G. A. Olah, *J. Am. Chem. Soc.*, 2003, **125**, 4836.
15 A. Schafer, H. Horn and R. Ahlrichs, *J. Chem. Phys.*, 1992, **97**, 2571.
16 F. Weigend, M. Haser, H. Patzelt and R. Ahlrichs, *Chem. Phys. Lett.*, 1998, **294**, 143.
17 A. Sodt, J. E. Subotnik and M. Head-Gordon, *J. Chem. Phys.*, 2006, **125**, 194109.
18 K. Eichkorn, O. Treutler, H. Öhm, M. Häser and R. Ahlrichs, *Chem. Phys. Lett.*, 1995, **240**, 283.
19 E. R. Davidson, *J. Comput. Phys.*, 1975, **17**, 87.
20 M. L. Leininger, C. D. Sherrill, W. D. Allen and H. F. Schaefer, *J. Comput. Chem.*, 2001, **22**, 1574.

21 Y. Notay, *SIAM J. Matrix Anal. Appl.*, 2006, **26**, 522.
22 R. Seeger and J. A. Pople, *J. Chem. Phys.*, 1977, **66**, 3045.
23 W. Lipscomb, *Acc. Chem. Res.*, 1973, **6**, 257.
24 W. Liang, Y. Shao, C. Ochsenfeld, A. T. Bell and M. Head-Gordon, *Chem. Phys. Lett.*, 2002, **358**, 43.
25 M. Sierka, A. Hogekamp and R. Ahlrichs, *J. Chem. Phys.*, 2003, **118**, 9136.
26 B. Dunlap, *J. Mol. Struct. (THEOCHEM)*, 2000, **501–502**, 221.
27 A. Sodt, G. Beran, Y. Jung, B. Austin and M. Head-Gordon, *J. Chem. Theor. Comput.*, 2006, **2**, 300.
28 Y. Shao, L. Fusti-Molnar, Y. Jung, J. Kussmann, C. Ochsenfeld, S. T. Brown, A. T. B. Gilbert, L. V. Slipchenko, S. V. Levchenko and D. P. O'Neill *et al.*, *Phys. Chem. Chem. Phys.*, 2006, **8**, 3172.
29 S. Saebo and P. Pulay, *Annu. Rev. Phys. Chem.*, 1993, **44**, 213.
30 C. W. Yoon and L. G. Sneddon, *J. Am. Chem. Soc.*, 2006, **128**, 13992.
31 G. Kodama, R. W. Parry and J. C. Carter, *J. Am. Chem. Soc.*, 1959, **81**, 3534.
32 C. E. Nordman and C. Reimann, *J. Am. Chem. Soc.*, 1959, **81**, 3538.
33 V. S. Nguyen, M. H. Matus, M. T. Nguyen and D. A. Dixon, *J. Phys. Chem. A*, DOI: 10.1021/jp0732007.
34 M. Sironi, M. Raimondi, D. L. Cooper and J. Gerratt, *J. Phys. Chem.*, 1991, **95**, 10617.
35 E. Switkes, R. M. Stevens and W. N. Lipscomb, *J. Chem. Phys.*, 1969, **51**, 2085.
36 W. T. Klooster, T. F. Koetzle, P. E. M. Siegbahn, T. B. Richardson and R. H. Crabtree, *J. Am. Chem. Soc.*, 1999, **121**, 6339.
37 L. R. Thorne, R. D. Suenram and F. J. Lovas, *J. Chem. Phys.*, 1983, **78**, 167.
38 R. D. Suenram and L. R. Thorne, *Chem. Phys. Lett.*, 1981, **78**, 157.
39 J. S. Binkley and L. R. Thorne, *J. Chem. Phys.*, 1983, **79**, 2932.
40 F. H. Stephens, R. T. Baker, M. H. Matus, D. J. Grant and D. A. Dixon, *Angew. Chem., Int. Ed.*, 2007, **46**, 746.
41 D. A. McQuarrie, *Statistical Mechanics*, University Science Books, Sausalito, CA, 2001.
42 J. E. Subotnik, A. D. Dutoi and M. Head-Gordon, *J. Chem. Phys.*, 2005, **123**, 114108.
43 J. E. Subotnik and M. Head-Gordon, *J. Chem. Phys.*, 2005, **122**, 034109.
44 A. C. Hurley, J. Lennard-Jones and J. A. Pople, *Proc. R. Soc. London, Ser. A*, 1953, **220**, 446.
45 W. J. Hunt, P. J. Hay and W. A. Goddard III, *J. Chem. Phys.*, 1972, **57**, 738.
46 W. A. Goddard III and L. B. Harding, *Annu. Rev. Phys. Chem.*, 1978, **29**, 363.
47 T. V. Voorhis and M. Head-Gordon, *Chem. Phys. Lett.*, 2000, **317**, 575.
48 W. Kohn, *Phys. Rev.*, 1959, **115**, 809.
49 S. Ismail-Beigi and T. A. Arias, *Phys. Rev. Lett.*, 1999, **82**, 2127.
50 E. Kapuy, Z. Csepes and C. Kozmutza, *Int. J. Quantum Chem.*, 1983, **23**, 981.
51 E. Kapuy, F. Bartha, F. Bogar, Z. Csepes and C. Kozmutza, *Int. J. Quantum Chem.*, 1990, **38**, 139.
52 E. Kapuy, F. Bogar and C. Kozmutza, *J. Mol. Struct.*, 1993, **297**, 365.
53 E. Kapuy, F. Bogar and E. Tfirst, *Int. J. Quantum Chem.*, 1994, **52**, 127.
54 J. Pipek and F. Bogar, *Top. Curr. Chem.*, 1999, **203**, 43.

